Research Square

Preprints are preliminary reports that have not undergone peer review.
They should not be considered conclusive, used to inform clinical practice,
or referenced by the media as validated information.

Assessment of isoprene epoxydiol reactive uptake onto acidic sulfate aerosols by real-time isomer characterization

Matthieu Riva

matthieu.n.riva@helsinki.fi

University of Helsinki https://orcid.org/0000-0003-0054-4131

Yuzhi Chen

Pacific Northwest National Laboratory

Manish Shrivastava

Pacific Northwest National Laboratory https://orcid.org/0000-0002-9053-2400

Peter Mettke

Leibniz Institute for Tropospheric Research https://orcid.org/0000-0002-3236-9780

Molly Frauenheim

University of North Carolina at Chapel Hill

Rebecca Rice

University of North Carolina at Chapel Hill

Brian Gaudet

Pacific Northwest National Laboratory

Jason Surratt

University of North Carolina at Chapel Hill https://orcid.org/0000-0002-6833-1450

Megan Claflin

Aerodyne Inc

Harald Stark

Aerodyne Inc

Stephan Graf

Tofwerk AG

Urs Rohner

Tofwerk AG

Laurent Poulain

Leibniz-Institut für Troposphärenforschung https://orcid.org/0000-0002-9128-7881

Hartmut Herrmann

Leibniz-Institut für Troposphärenforschung https://orcid.org/0000-0001-7044-2101

Sebastian Gerber

Tofwerk AG

Felipe Lopez-Hilfiker

Tofwerk AG

Avram Gold

University of North Carolina at Chapel Hill https://orcid.org/0000-0003-1383-6635

Michael Kamrath

Tofwerk AG

Vasyl Yatsyna

Tofwerk AG https://orcid.org/0000-0002-3112-4298

Article

Keywords:

Posted Date: October 16th, 2026

DOI: https://doi.org/10.21203/rs.3.rs-11300884/v1

License: This work is licensed under a Creative Commons Attribution 4.0 International License. Read Full License

Additional Declarations: Yes there is potential Competing Interest. M.R., V.Y., S.Gr., S.G., U.R., F.L. and M.Z.K. work for Tofwerk AG, and M.C. and H.S. work for Aerodyne Research Inc., companies that commercialize the Vocus-IMS mass spectrometer. MOBILion is the exclusive licensee of the SLIM technology for commercialization purposes; Tofwerk has been authorized to implement the proprietary technology in select products. The other authors declare no competing interests.

Assessment of isoprene epoxydiol reactive uptake onto acidic sulfate aerosols by real-time isomer characterization

M. Riva[1,2,†,*], Y. Chen[3,†], M. Shrivastava[3], P. Mettke[4], M. P. Frauenheim[5], R. L. Rice[5], B. Gaudet[3], J. D. Surratt[5,6], M. Claflin[7], H. Stark[7], V. Yatsyna[1], S. Graf[1], U. Rohner[1], L. Poulain[4], H. Herrmann[4], S. Gerber[1], F. Lopez-Hilfiker[1], A. Gold[5,*], M. Z. Kamrath[1,*]

[1] Tofwerk, 3645 Thun, Switzerland.

[2] Institute for Atmospheric and Earth System Research (INAR) /Physics, University of Helsinki, Helsinki, Finland.

[3] Pacific Northwest National Laboratory, Richland, Washington 99354, United States.

[4] Atmospheric Chemistry Department (ACD), Leibniz Institute for Tropospheric Research (TROPOS), Leipzig, Germany.

[5] Department of Environmental Sciences and Engineering, Gillings School of Global Public Health, University of North Carolina at Chapel Hill, Chapel Hill, North Carolina 27599, United States.

[6] Department of Chemistry, College of Arts and Sciences, University of North Carolina at Chapel Hill, North Carolina 27514, United States.

[7] Aerodyne Research Inc., Billerica, Massachusetts 01821 United States.

†These authors contributed equally.

*Correspondence: matthieu.n.riva@helsinki.fi; golda@email.unc.edu; Michael.Kamrath@tofwerk.com

Abstract

Isoprene epoxydiols (IEPOX) are key precursors of secondary organic aerosol (SOA) in isoprene-rich regions, yet their multiphase chemistry and gas–particle partitioning remain poorly constrained. Here we combine real-time isomer speciation by ion mobility–chemical ionization mass spectrometry with a zero-dimensional kinetic box model to constrain the reaction kinetics and volatility of major non-sulfated IEPOX-derived SOA constituents. Chamber experiments reveal substantial acid-driven, particle-phase IEPOX isomerization on sulfate aerosols, yielding 3-methylenebutane-1,2,4-triol and 3-methyltetrahydrofuran-2,4-diols that partition preferentially to the gas phase. Their experimentally derived volatilities are substantially higher than previously assumed. Although these volatile products can form SOA upon gas-phase oxidation, their contribution to isoprene-derived SOA in the Amazon Basin and the southeastern United States is limited. Implementing the updated rate constants and volatilities in WRF-Chem lowers simulated IEPOX-derived SOA by up to 65% in the Amazon Basin and up to 21% in the southeastern United States relative to the base case, indicating that other chemical or biological processes contribute to ambient IEPOX-derived SOA. This framework provides a more physically and chemically consistent basis for predicting isoprene-derived SOA, with implications for air quality and climate projections.

Introduction

Secondary organic aerosol (SOA) formed through the oxidation of volatile organic compounds (VOCs) is a major and globally ubiquitous component of atmospheric fine particulate matter ($PM_{2.5}$; aerosol particles ≤ 2.5 μm in aerodynamic diameter)[1]. Aerosol chemical composition and physicochemical properties, such as viscosity and phase state, play a central role in the effects of SOA on air quality and climate[1,2]. Understanding how SOA forms and evolves is crucial to accurately evaluating its importance in the Earth's climate system and adverse effects on public health.

Isoprene (2-methyl-1,3-butadiene) is the dominant biogenic VOC, with global emissions of approximately 450 Tg C yr^{-1},[3] representing ~38% of the total VOC flux[4–6]. Under sub-ppb level of nitric oxide, isoprene oxidation by hydroxyl (OH) radicals yields a suite of products, with isoprene epoxydiols (IEPOX; $C_5H_{10}O_3$) as the major second-generation gas-phase oxidation products (up to 70% yield), and primarily as the 2,3-epoxide isomers with the *trans- and cis-* isomers predominating (*trans-*/*cis-*β-IEPOX; 97%)[5]. Accordingly, laboratory studies have demonstrated that acid-driven multiphase chemistry (or reactive uptake) of IEPOX is key to explaining the chemical form and extent of SOA formation from photochemical oxidation of isoprene[5,7–9]. Field measurements have confirmed that this is the predominant pathway forming isoprene-derived SOA, contributing up to 40% of submicron organic aerosol mass[10–14]. As isoprene emissions increase due to warming, and NO_x and SO_2 emissions decline with the implementation of air quality regulations, efficiency of IEPOX uptake to form submicron SOA mass is expected to rise[15].

Chamber studies have shown that 2-methyltetrols and organosulfur compounds, specifically organosulfates (OS) formed by the reactive uptake of IEPOX onto particulate SO_4^{2-}, contribute significantly to IEPOX-derived SOA[7,16–18]. In addition to OS and 2-methyltetrols, IEPOX uptake onto particulate sulfate yields newly-resolved $C_5H_{10}O_3$ isomers, including 3-methylenebutane-1,2,4-triol and 3-methyltetrahydrofuran-2,4-diols, through acid-driven particle-phase IEPOX isomerization[19,20]. Initially considered analytical artifacts formed during thermal analysis of SOA, recent evidence suggests these $C_5H_{10}O_3$ represent a potentially important mass fraction of IEPOX reactive uptake products[20], which upon partitioning into the gas phase can form substantial amounts of SOA by atmospheric OH oxidation (i.e., 1.95 ± 0.81 Tg C yr^{-1} and 1.76 Tg C yr^{-1} for 3-methylenebutane-1,2,4-triol and 3-methyltetrahydrofuran-2,4-diol, respectively)[21]. However, current analytical protocols and instrument biases have limited real-time quantitative assessment of their atmospheric relevance.

Although online gas-phase mass spectrometry techniques such as chemical ionization mass spectrometry (CIMS) have advanced substantially, enabling elemental formula-based detection, conventional CIMS approaches cannot resolve isomers[22,23]. Furthermore, structure-dependent sensitivity of CIMS can vary by orders of magnitude, biasing detection toward the most efficiently ionized structures regardless of their

actual abundance. As a result, models often oversimplify IEPOX reactive uptake as irreversible and fail to capture contributions from semi-volatile products such as the multiple $C_5H_{10}O_3$ species[20,24,25], leading to inaccurate prediction of the formation of isoprene-derived SOA. By using offline techniques, Frauenheim et al.[20] notably resolved the additional $C_5H_{10}O_3$ isomers 3-methylenebutane-1,2,4-triol and 3-methyltetrahydrofuran-2,4-diols, which can partition into the gas phase and undergo subsequent atmospheric OH oxidation to then yield previously unrecognized SOA[21]. To address these limitations, we employed low-pressure ion mobility spectrometry coupled with chemical ionization time-of-flight mass spectrometry (Vocus CI-IMS-TOF) to achieve real-time isomer separation. Using authentic standards, we identified key IEPOX-derived semivolatile $C_5H_{10}O_3$ isomerization products and quantified their formation during acid-driven multiphase reactions. Our laboratory results, combined with box model simulations, provide updated parameterizations for regional-scale modeling, yielding improved predictions of isoprene-derived SOA formation. Our findings underscore the importance of isomer-specific detection of acid-driven particle-phase IEPOX isomerization products in constraining the atmospheric fate of reactive oxidation products and establish a new framework for modeling one of the most efficient oxidation pathways in SOA production.

Results

Isomer-resolved detection of IEPOX uptake products

Chemical ionization coupled with high-resolution mass spectrometry reliably analyzes VOCs in a variety of environments[22,23]. However, isomeric, or in certain cases, isobaric structures present ambiguity in analysis, as there is no definitive measurement of the structures contributing to the intensity of a mass signal. This remains a continuing issue in atmospheric chemistry. Notably, from the OH-initiated oxidation of isoprene, primary and secondary gas-phase oxidation products such as isoprene hydroxy hydroperoxide (ISOPOOH) and IEPOX share the same molecular formulae ($C_5H_{10}O_3$)[5,6], making it challenging to retrieve the contribution/dynamics of such reactive species. As indicated above, Frauenheim et al.[20] recently revealed the formation of additional $C_5H_{10}O_3$ compounds, including 3-methylenebutane-1,2,4-triol (triol) and 3-methyltetrahydrofuran-2,4-diols (THF-diols). Despite the wealth of studies on the reactive uptake of IEPOX, the formation of its in-particle isomerization products (triol and THF-diols) remains to be fully constrained by using real-time CIMS techniques. We performed controlled chamber experiments in the presence of ammonium bisulfate (ABS) seed particles (pH = 1.5) at approximately 30 % relative humidity (RH), where either *trans*- or *cis*-*β*-IEPOX was injected, and gas-phase products were resolved using the Vocus CI-IMS-TOF. Experiments were performed in triplicate and present good reproducibility in IEPOX-derived SOA formation (+/- 18% by mass) as depicted in Supplementary Fig. 1. This run-to-run variability most likely reflects small differences in IEPOX injection efficiency (i.e., 0.78 and 0.90 for *trans*- or *cis*-*β*-IEPOX, respectively, see Methods), and seed particle surface area between experiments (Supplementary Fig. 1).

Supplementary Fig. 2 shows that the Vocus CI-IMS-TOF offers an overall efficient separation of the isomeric $C_5H_{10}O_3$ products. The sensitivity of each product ion was determined (Supplementary Table 1), enabling an accurate quantitation of its formation during the reactive uptake of IEPOX in the presence of ABS seed particles. As shown in Fig. 1, the time-resolved isomer speciation allowed us to deconvolute the consumption of the precursor and the formation of the uptake products sharing the same molecular composition. The upper panel of Fig. 1a demonstrates that immediately following the injection of ABS particles, a rapid depletion of *trans*-β-IEPOX was observed leading to virtually complete consumption. Time series traces of gas phase $C_5H_{10}O_3$ show a sharp rise in semivolatile rearrangement products, consistent with acid-driven ring-opening and rearrangement pathways occurring in the aqueous particle phase. For the uptake of *cis*-β-IEPOX(Fig. 1b), it should be noted that the Vocus CI-IMS-TOF does not resolve *cis-β*-IEPOX and 3-methylenebutane-1,2,4-triol, which explains the persistence of the trace corresponding to *cis-β*-IEPOX composition ($C_5H_{10}O_3$). As a result, the concentration of 3-methylenebutane-1,2,4-triol was calculated by assuming the total consumption of *cis-β*-IEPOX as observed during the acid-driven uptake of *trans-β*-IEPOX.

On average, the gas-phase $C_5H_{10}O_3$ reactive uptake products (Fig. 1 and Supplementary Figs. 3 and 4) represent ~ 21% of reacted IEPOX and demonstrate a subsequent partitioning into the gas phase following their in-particle formation through IEPOX isomerization. 2-Methyltetrols were also observed in the gas phase and suggested similar gas partitioning (Supplementary Fig. 5), but to a lesser extent, which was expected due to the reduced volatility.

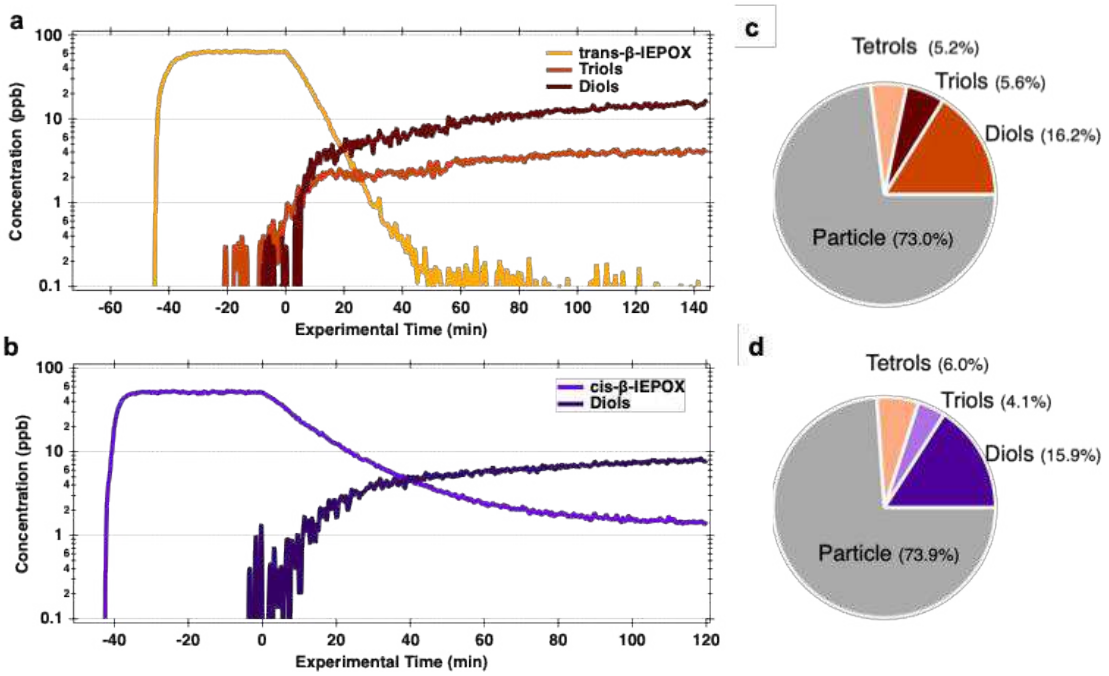


Fig. 1: Isomer-resolved gas-phase products of IEPOX reactive uptake onto acidic sulfate seed. a,b Evolution of the gas-phase isomeric $C_5H_{10}O_3$ compounds, including 3-methylenebutane-1,2,4-triol (triol) and the 3-methyltetrahydrofuran-2,4-diols (THF-diols), during the reactive uptake of (**a**) *trans*- and (**b**)

cis-β-IEPOX; t = 0 corresponds to the injection of seed particles. **c,d** Distribution of IEPOX mass between the gas and particle phases at equilibrium (~180 min), showing the fraction of IEPOX-derived carbon partitioned to the gas phase. The particle fraction corresponds to IEPOX that forms low-volatility products, including 2-methyltetrols, organosulfates and oligomers.

The higher particle volume concentrations used during chamber experiments (100-150 $\mu m^3\ cm^{-3}$) promote partitioning into the particle phase compared to more dilute ambient conditions. This would result in a shift in the gas-to-particle phase equilibrium. Thus, for semi-volatile species, such as the $C_5H_{10}O_3$ reactive uptake products, the extent of partitioning into the gas phase following in-particle formation is likely a lower limit. In other words, under more dilute atmospheric environments, and including partitioning of the tetrols (Supplementary Fig. 5), it can be expected that more than 25% of the IEPOX reactive uptake compounds can partition back to the gas phase.

Box-model constraints on kinetics and volatility

To assess the influence of partitioning on IEPOX reactive uptake, we constrained the THF-diols and triol formation kinetics using a zero-dimensional, time-dependent chemical kinetic box model[24,26]. The model simulates gas-phase IEPOX uptake by ABS seed particles through a pseudo-first-order decay and includes semi-explicit aerosol-phase tracer formation (Methods). While recent IEPOX SOA parameterizations account for inorganic–organic phase separation and diffusion limitations in the $IEPOX_{(g)}$–aerosol heterogenous reaction probability (γ_{IEPOX})[15,25,27], these were omitted here for simplicity. Instead, a constant γ_{IEPOX} was prescribed for each experiment to match measured gas-phase IEPOX decay (Supplementary Fig. 6) as gas-phase diffusion becomes rate-limiting only for uptake coefficients approaching unity. As a result, the γIEPOX values derived here remain well below this regime, supporting the use of a constant uptake coefficient and ensuring accurate particle-phase uptake estimates. To match chamber observations, THF-diol and triol formation rates were multiplied by 62 and 5, respectively (Supplementary Tables 2 and 3). The discrepancy primarily arises from previous studies not accounting for the gaseous partitioning of IEPOX-derived isomerization products[24,27,28]. In addition, the vapor pressure (C*) of 2-methyltetrols was updated from 10 to 35 $\mu g\ m^{-3}$. This revised value was used to vary, together with the R2–R4 rate constants, when fitting the box model to the measured gas-phase THF-diol, triol, 2-methyltetrols, and total OA time series described above, rather than being adopted directly from an independent literature source. Vapor pressures of the THF-diols and triol were determined as 1.6×10^4 and 521 $\mu g\ m^{-3}$, respectively (Supplementary Table 4). The rate for tetrol formation agrees with recent estimates for 2-methyltetrols[24,29–32], and indicate that THF-diol and triol volatility was substantially underestimated in earlier work[20,33,34]. These values differ from vapor pressure estimates for the same isomerization products generated with the U.S. EPA OPERA model (i.e., 1687 and 2297 $\mu g\ m^{-3}$ for triol and diol, respectively)[19], which are approximately 7-fold lower for the diol and 3-fold higher for the triol than our box-model-derived values. This discrepancy reflects the different estimation methods (group-contribution vapor pressure model versus EPA OPERA) and underscores the sensitivity of predicted

IEPOX-SOA yields to the volatility parameterization used. Overall, the box model reproduced the observed IEPOX reactive uptake products and OA mass (Fig. 2a), supporting the updated parameterization. The model was designed to reproduce the observed products and not to match the product formation rate (i.e., constant γ_{IEPOX} Methods); parameterizations that explicitly resolve diffusion limitations and inorganic–organic phase separation would be expected to slow the early-time rise[31]. In addition, the time delay between the model and observations may also be explained by passivation of the sampling line, which has been shown to delay and bias measurements of semivolatile and intermediate-volatility species[35]. This approach provides a more accurate representation of IEPOX-derived SOA formation by accounting for acid-driven particle-phase IEPOX isomerization that yields the diols and the triol, followed by their off gassing. Hence, partitioning analysis suggests THF-diols remain in the gas phase and triols substantially partition to the gas phase, while 2-methyltetrols remain substantially in the particle phase (Fig. 2). Overall, ~70% of the quantified mass resides in particles, with 2-methyltetrols, OS, and dimers as the principal constituents, consistent with prior studies[6,15–17].

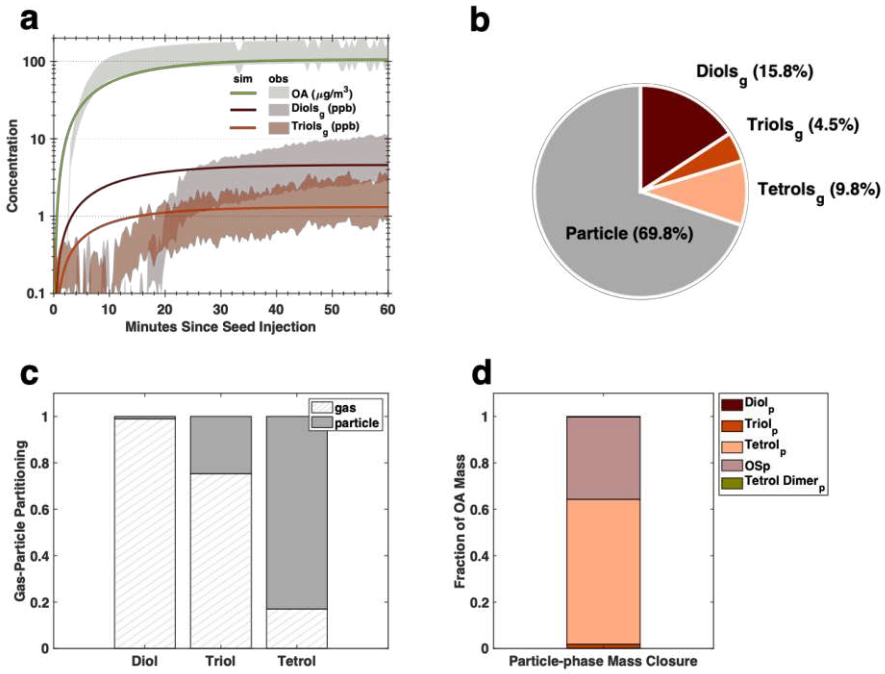


Fig. 2: Box-model constraints on IEPOX uptake and product partitioning. a Fit of the OA mass and gas-phase THF-diol and triol observations (shaded areas reflect an uncertainty factor of 2 from the measured values). **b** Fate of IEPOX. **c** Gas–particle partitioning of semivolatile species, including THF-diols, triol and 2-methyltetrols. **d** Particle-phase product distribution for *trans*-*β*-IEPOX experiment #2.

Implications for regional IEPOX-derived SOA

To evaluate the broader implications of the laboratory findings, we incorporated the new rate constants and volatility estimates from the chemical kinetic box model into the Weather Research and Forecasting model coupled with Chemistry (WRF-Chem) to simulate IEPOX-derived SOA formation and SOA

formation from OH initiated oxidation of diols and triols. High-resolution WRF-Chem simulations were performed at 10–12 km grid spacing, resolving cloud processes, chemistry, and emissions for the GoAmazon2014/5 and SOAS 2013 campaigns. Simulations covered 21–29 September 2014 for GoAmazon and 20–28 June 2013 for SOAS, with the first three days used for aerosol and trace gas spin-up. The modeled domains encompassed the Amazon Basin and the southeastern United States, respectively (Methods). Due to the computational cost of the SOA parameterizations and high-resolution runs, simulations were limited to one week. Nevertheless, results are expected to be broadly representative, as both observations and prior WRF-Chem studies indicate that sharp plume–background oxidant contrasts are a persistent feature across multiple days[36].

IEPOX-derived SOA formation was simulated using a heterogeneous reactive uptake scheme based on a resistor model[37], which accounts for gas-phase diffusion, surface accommodation, diffusion through an organic shell surrounding an aqueous inorganic core, and particle-phase reactions leading to key IEPOX-derived SOA components. The scheme also represents reversible partitioning of 2-methyltetrols between the gas and particle phases, as well as their oligomerization into nonvolatile products[38–40]. Finally, these simulations now resolve SOA formation through the OH-initiated oxidation of THF-diol and triol (Sim 1 and Sim 2, unlike the default case). THF-diol+triol SOA (Supplementary Figs. 11c, 12c and 13c) accounts for 5.0% and 4.1% of total simulated IEPOX-SOA in the SE US (Sim 1 and Sim 2, respectively) and 0.21% and 0.11% in the Amazon (Supplementary Fig. 14). Regionally, particle-phase IEPOX-SOA therefore remains dominated by 2-methyltetrols, 2-methyltetrol sulfates, and high molecular weight compounds.

Supplementary Table 5 lists WRF-Chem sensitivity simulations varying IEPOX-SOA formulations conducted in this study. Figs. 3a,d show the default simulation using the parameterization described by Shrivastava et al.[36] which does not include THF-diol and triol formation in the particle phase and assumes a 2-methyltetrol C* value of 10 μg m^{-3} based on a previous study[34]. The oligomerization of 2-methyltetrols was turned off in all simulations (default, Sim 1 and Sim 2) due to extremely long timescales (~1000 hours) estimated for their oligomerization from box model simulations in this study. Compared to the default simulation, incorporating the new laboratory-derived parameters (Sim 1), which includes THF-diol and triol formation and a methyltetrol C* value of 35 μg m^{-3} resulted in a net reduction of IEPOX-derived SOA in both the southeastern U.S. (Fig. 3, top panels) and Amazon Basin (Fig. 3, bottom panels). The largest effect occurs in the Amazon Basin, where direct emissions of 2-methyltetrols from the vegetation were reported[41]. Combined with the greater than expected volatility of 2-methyltetrol gases determined here and supported by recent studies[42] this led to a 40–60% decrease in simulated IEPOX-derived SOA formation (Fig. 3f). In the southeastern U.S., where no direct emissions of 2-methyltetrols have been demonstrated (direct emissions of 2-methyltetrols were not incorporated in WRF-Chem for SE USA), the reduction is smaller but can still reach up to 20% (Fig. 3c).

Additional simulations were conducted using a vapor pressure of 2-methyltetrol consistent with previous studies (C*, 10 μg m^{-3})[34], but with THF-diol and triol formation incorporated from this study to isolate the role of the THF-diols and triol in IEPOX-derived SOA formation. As shown in Supplementary Fig. 9, the resulting reduction in SOA formation is modest, ranging from 2–10% in the SE-US (Supplementary Fig. 9c) and up to 5% in the Amazon Basin (Supplementary Fig. 9f). This minor impact aligns with our laboratory findings; THF-diols, major IEPOX-derived isomerization products, are expected to remain entirely in the gas phase under atmospherically relevant conditions. Therefore, the largest impact on IEPOX-SOA formation is due to change in the 2-methyltetrol C* value from 10 μg m^{-3} (default) to 35 μg m^{-3} (revised in Fig. 3). It should be noted that the rate constants derived from laboratory experiments correspond to RH < 50% and acidic aerosol particles. To represent higher RH and less acidic aerosol conditions than the pH 1.4–1.5 seed used in the chamber experiments, ambient SOAS and GoAmazon particles remain acidic (pH roughly 0–2), $k_{THF\text{-}diols}$ (R2) and k_{triols} (R3) were scaled down by ~ 13-fold in the same manner as $k_{tetrols}$ reported in the literature[27], under the assumption that THF-diol and triol formation would be similarly suppressed. To evaluate the sensitivity to this assumption, additional WRF-Chem simulations were performed for the SE-US with higher $k_{THF\text{-}diols}$ and k_{triols} while maintaining a C* value of 35 μg m^{-3} for 2-methyltetrols. As depicted in Supplementary Fig. 10c, this leads to a more pronounced reduction in IEPOX-derived SOA formation (Supplementary Fig. 10c compared to Supplementary Fig. 9c), ranging from 5% to 25%. Although Frauenheim et al.[21] demonstrated that SOA can form from the OH oxidations of the THF-diols and triol, the simulations performed here suggest that these chemical processes will have a negligible impact on isoprene-derived SOA formation.

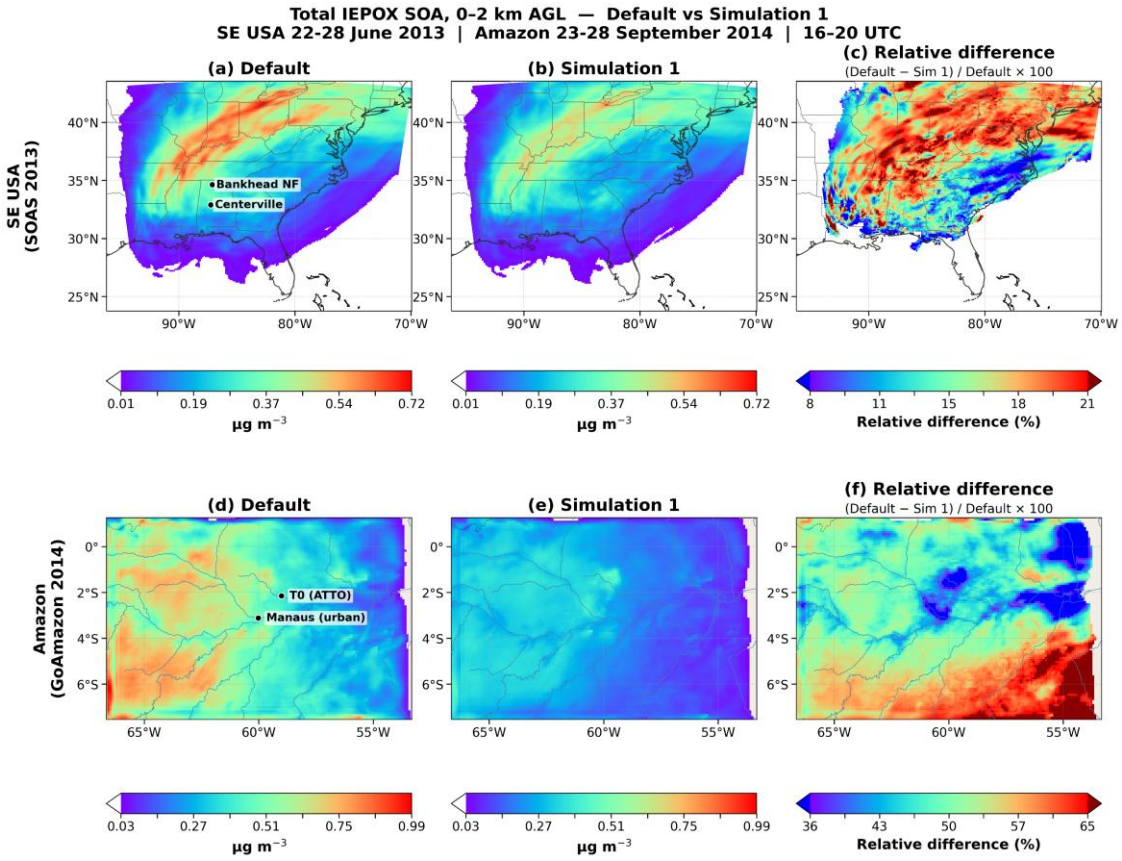


Fig. 3: WRF-Chem-simulated spatial distributions of IEPOX-derived SOA. Near-surface-layer (0–2 km altitude) IEPOX-SOA concentrations (µg m^{-3}) are shown for the default parameterization (left panels) and the updated parameterization derived from the chemical kinetic box model (middle panels). The relative difference between the two simulations is shown in percent (right panels). **a–c** Simulations over the southeastern United States (20–28 June 2013). **d–f** Simulations over the Amazon Basin (21–29 September 2014).

Comparison with field-derived IEPOX-SOA

As a first-order check on the absolute magnitude of these predictions, we compared the domain- and time-averaged (16–20 UTC, 0–2 km AGL) simulated IEPOX-SOA against published field-based estimates for both regions within the same dates. At both sites, the simulation underpredicts the field-derived Isoprene-OA/IEPOX-OA PMF factor, but by very different margins. At Centreville, the period-average simulated concentration (~0.35 µg m^{-3}) is roughly 40% lower than the Xu et al.[14] isoprene-OA value (~0.6 µg m^{-3}). At the Amazonian T3 site the gap is far larger: the model (~0.30 µg m^{-3}) captures only about one-tenth of reported IEPOX-SOA value (~2.7 µg m^{-3})[43]. Part of this disparity, particularly at T3, may not reflect a deficiency in the simulated acid-driven IEPOX uptake chemistry itself, but rather a mismatch between what the field PMF factor represents and what the model specifically simulates. Even at the source, the AMS-PMF "Isoprene-OA"/IEPOX-SOA factor is not a pure IEPOX-SOA signal: Hu et al.[13] showed that explicit IEPOX-derived molecular tracers (2-methyltetrols, triols, IEPOX-organosulfates) account for ~78% of the PMF-resolved factor mass at SOAS/Centreville, and Zhang et al.[33] demonstrated, using a

field-data-constrained CMAQ scheme evaluated against six orders of magnitude in observed 2-methyltetrol/2-methylglyceric acid concentrations, that the classic acid-driven multiphase (IEPOX) pathway alone cannot reproduce observed marker abundances without additional chemical or biological processes, including non-aqueous formation, direct biogenic emission, or cloud processing. For example, over the Amazon specifically, Shrivastava et al.[39] found that incorporating direct emissions of 2-methyltetrols, reflective of the latest estimates of in-plant and surface biochemistry, significantly reduced the discrepancy in fine particulate mass between model and aircraft measurements in the upper troposphere over the Amazon rainforest. While this suggests that direct biogenic emission is a promising pathway the dependence of these biological processes and associated emission rates on plant type and environmental stressors remains uncertain and additional measurements are needed to develop process-level understandings and constrain model parameterization[41]. Overall, these findings suggest that the field-observed Isoprene-OA/IEPOX-OA signal, especially at T3, reflects contributions from biogenic and chemical SOA-forming pathways beyond the acid-driven reactive uptake process of IEPOX captured here, convolved with the IEPOX-SOA tracer signature in AMS-PMF analysis. This does not close the full model–observation gap, but it narrows the fraction of the discrepancy that can be fairly attributed to errors in the IEPOX reactive-uptake parameterization alone.

Discussion

This study integrates laboratory-derived kinetic and volatility constraints into a multiphase chemical framework to improve the representation of IEPOX-derived SOA formation in atmospheric models. Box model simulations of IEPOX uptake constrained by real-time speciation into THF-diol and triol isomers and 2-methyltetrols reveal that approximately 25% of the initial IEPOX mass partitions back to the gas phase, with THF-diols remaining entirely in the gas phase and triols having an overall minor impact on gaseous composition under atmospherically relevant conditions. The measured volatilities of the major IEPOX reactive uptake products significantly reduce modeled IEPOX-SOA yields compared to previous parameterizations. When implemented in WRF-Chem, the updated parameters result in a substantial decrease in IEPOX-SOA formation compared to the base model: 40–65% in the Amazon Basin, where direct biogenic emissions of 2-methyltetrols might be significant, and up to 21% in the southeastern U.S. Sensitivity simulations confirm the dominant role of 2-methyltetrol volatility, with THF-diols and triols exerting only a minor influence on SOA mass under typical atmospheric conditions. These findings suggest that earlier studies may have overestimated IEPOX-derived SOA burdens due to the omission of gaseous partitioning and the use of underestimated volatility values.

Given the central role of 2-methyltetrol volatility in these results, further constraining its sources and volatility represents a key priority for improving predictions of isoprene-derived SOA formation. By reconciling laboratory observations with regional-scale modeling, this work provides a more physically and chemically consistent description of IEPOX-derived SOA formation, likely improving predictive capability for both present-day air quality and future climate scenarios. More broadly, the acid-driven

IEPOX chemistry may not be unique to this system: other reactive-uptake products with similarly under constrained volatility could be subject to comparable in-particle isomerization and subsequent gas-phase repartitioning, a possibility that, to our knowledge, remains largely unexplored and underscores the broader relevance of the work presented here.

Methods

Smog chamber experiments

Experiments were conducted in the Atmospheric Chemistry Department Chamber (ACD-C) of the Leibniz Institute for Tropospheric Research (TROPOS) in Leipzig, Germany. The 19 m^3 cylindrical chamber is made of fluorinated ethylene propylene with a surface-to-volume ratio of about 2.1 and enclosed in a temperature-controlled housing. Before each experiment, the chamber was flushed for at least 16 h with 200 L min^{-1} purified air. The relative humidity (RH) was brought to and kept constant at 35 ± 3 % RH and 21 ± 2 °C by nebulizing MilliQ water injected through a capillary into a sufficiently heated compressed air tube flushing the chamber, using an HPLC-pump (Merck Hitachi L-6200). During the experiments, a fan was used to ensure proper mixing in the chamber. Temperature and RH were measured by a probe (HMT330; Vaisala, Vantaa, Finland). Monitors for ozone (49C Ozone Analyzer, Thermo Scientific, USA) and NO_x (42i TL Trace Level NO_x Analyzer, Thermo Scientific, USA) measured the respective trace gas levels. VOC concentrations were monitored using a Proton Transfer Reaction Time-of-Flight Mass Spectrometer (PTR-ToF-MS, Ionicon, Innsbruck, Austria)[44]. The particle number-size distribution was measured by a TROPOS-style Mobility Particle Size Spectrometer (MPSS)[45]. Reactive uptake experiments were performed with authentic standards and the atmospheric simulation chamber operated in batch mode. After the desired RH was reached, the exhaust was closed and 50 µL of a 100 mg mL^{-1} solution of the respective synthesized standard in acetonitrile (≥99.9 %, Riedel-de-Haën) was injected by syringe through a septum in the main gas flow. To ensure full evaporation, flushing of the injection port was continued for 300 s after the injection, before the flushing was stopped, which marked the start of the experiment. To determine the injection efficiency, acetonitrile was quantified using the PTR-ToF-MS. To monitor the wall loss of IEPOX, a blank period was recorded for 40 min. After that, seed particles were generated by spraying a suitable particle stock solution through a nozzle and injected without drying into the humidified stream of compressed air of 200 LPM for 300 s. Two stock solutions were used in this study, a high acidity seed solution (pH 1.4, i.e., ABS) of 7.93 g L^{-1} $(NH_4)_2SO_4$ (Merck Millipore) and 3.3 mL L^{-1} H_2SO_4 (Sigma Aldrich) and a medium acidity seed solution (pH 3, i.e., AS) of 15.5 g L^{-1} $(NH_4)_2SO_4$ and 0.13 mL L^{-1} H_2SO_4.

To better assess the underlying sources and sinks, gas-phase concentrations were corrected for wall loss based on the *trans*- and *cis*-*β*-IEPOX decay rates measured once the precursor was injected into the chamber, prior to seed particle injection. Therefore, the 40 min before particle injection was treated as the reference period, assuming wall loss to be the only sink for gas-phase compounds. The first-order rate

constant was calculated for that period and treated as the wall-loss rate throughout the experiment. For every time step, the corresponding wall-loss fraction was calculated and subsequently added to the original gas-phase signal. To avoid overestimation of the original gas-phase concentration of compounds with pronounced uptake behavior after the seed injection, the wall-loss correction was only applied until the uptake process was finished for these compounds.

Vocus chemical ionization ion mobility mass spectrometer

When distinct isomers need to be resolved, ion mobility spectrometry (IMS) is a technique that can be used in conjunction with mass spectrometry. IMS discriminates between ions that adopt structures that differ in their rotationally averaged collision cross sections (i.e., average molecular size). With the low-pressure IMS coupled to a Vocus chemical ionization time of flight mass spectrometer (Vocus CI-IMS-TOF, TOFWERK AG), analytes are ionized by chemical ionization with an iodide adduct ionization mechanism (AIM) reactor[46]. Iodide reagent ions are generated by a compact Vacuum Ultra-Violet (VUV) ion source in which a constant amount of benzene (i.e., photo-absorber) and methyl iodide is delivered by passing 0.250 slpm UHP nitrogen stream through a permeation tube held at 80 °C. Once produced, iodide reagent ions form an adduct with the gas-phase analytes within the AIM reactor operated at 50 mbar and 50 °C. The resulting ions are then separated through collisions with the buffer gas in the IMS chamber at reduced pressure before mass analysis. This provides two-dimensional information—the mass-to-charge ratio and ion mobility drift time. This deconvolutes multiple isomeric or isobaric components present in a single mass spectrum peak. The IMS separation chamber is purged with an inert buffer gas (e.g., helium) and maintained at a pressure of 3.80 mbar. The ions are moved along a 9-meter serpentine path using technology developed at Pacific Northwest National Laboratory for lossless ion manipulations (SLIM)[47]. The movement of ions is controlled using weak electric fields and radiofrequency. Ions with small collision cross sections have fewer interactions with the buffer gas and arrive at the end of the drift region sooner than ions with larger collision cross sections. The total time an ion spends traveling through the IMS drift region is referred as the IMS drift time, which is related to a molecule's collision cross section. IMS mode allows for the individual components of a single mass peak to be separated. When product ions are directed into the mobility region, a pseudorandom sequence (multiplexing) is applied to the ion gate, modulating the ion signal, and providing critical timing information to measure drift times. Due to ion modulation, ion losses are evident when comparing the IMS-MS mass spectrum to the MS-only mass spectrum. Based on the 50% duty cycle of the gate sequence, the theoretical expectation is to measure 50% of the ion signal in IMS-MS mode relative to MS-only mode. Experimentally, 40% of the ion signal is measured in IMS-MS mode compared to MS-only mode—a 10% difference between theory and experiment indicating that a small percentage of ions are lost either in the drift region or at the ion gate.

Calibration of the Vocus CI-IMS-MS

To measure the instrument sensitivity and retrieve drift times of the IEPOX isomers and the $C_5H_{10}O_3$ reactive uptake products, we calibrated the reactor using authentic standards synthesized following published procedures developed at at the University of North Carolina at Chapel Hill with purity confirmed by NMR and mass spectrometry. *Cis* and *trans β*-IEPOX,[48] 3-methylenebutane-1,2,4-triol, 3-methyltetrahydrofuran-3,4-diol,[19] 3-methyltetrahydrofuran-2,4-diol,[19] and 2-methyltetrols[43] were each dissolved in acetonitrile solution and a liquid calibration system (LCS v2, Tofwerk) was then used to form standard concentrations ranging from 20 to 80 ppb. By introducing a continuous flow of solution of known concentration into a nebulizer and aluminum evaporation chamber, the LCS provides a continuous, calibrated gas-phase concentration to the instrument. The evaporation chamber of the LCS was set to a temperature of 200 °C, with a UHP nitrogen flow rate of 2000 slpm, thereby slightly overflowing the sample inlet. For the different isoprene oxidation products, we cannot rule out losses in the LCS, but find that sensitivities for IEPOX are in good agreement with previous work[49]. Aqueous solutions with concentrations ranging from 5 to 50 μM and liquid flow rates of 5-30 μL/min were used to reach stable and reliable signals for IMS drift time characterization.

Box-modeling study

We constrained the reaction kinetics of THF-diols and triols formation using a zero-dimensional time-dependent chemical reaction kinetic box model[24]. Briefly, the box model simulates gas-phase IEPOX uptake by acidic sulfate aerosol through a pseudo-first-order decay (R1) and includes semi-explicit aerosol-phase tracer formation (R2–R6; described below). The pseudo-first-order heterogeneous reactive uptake rate constant (k_{het}) was calculated by Eqn. (1):

$$k_{het} = \gamma_{IEPOX} S_a \omega / 4 \quad (1)$$

where γ_{IEPOX} is the $IEPOX_{(g)}$–aerosol heterogenous reaction probability or reactive uptake coefficient, ω (cm/s) is the mean molecular speed of IEPOX vapor, and S_a is the total aerosol surface area concentration ($cm^2\ cm^{-3}$).

$$IEPOX_{(g)} \xrightarrow{k_{het}} IEPOX_{(aq)} \quad (R1)$$

$$IEPOX_{(aq)} + H^+ \rightarrow Diols + H^+ \quad (R2)$$

$$IEPOX_{(aq)} + H^+ \rightarrow Triols + H^+ \quad (R3)$$

$$IEPOX_{(aq)} + H^+ + H_2O \rightarrow Tetrols + H^+ \quad (R4)$$

$$IEPOX_{(aq)} + H^+ + SO_4^{2-} \rightarrow Tetrol\ Sulfate\ (OS) \quad (R5)$$

$$IEPOX_{(aq)} + H^+ + Tetrols \rightarrow Tetrol\ Dimers \quad (R6)$$

The initial molar concentrations of aerosol inorganic species ($[NH_4^+]$, $[H^+]$, $[H_2O]$, $[HSO_4^-]$, $[SO_4^{2-}]$) and total aqueous aerosol-phase volume were obtained from the Extended AIM Aerosol Thermodynamic

Model II (http://www.aim.env.uea.ac.uk/aim/aim.php)[50,51] with inputs of the atomizer solution composition, measured temperature and relative humidity of the chamber. Once in the aerosol phase, IEPOX was allowed to undergo acid-driven reactions forming the THF-diols, triol, 2-methyltetrols, 2-methyltetrol sulfates, and high molecular weight compounds including methyltetrol and methyltetrol sulfate dimers. Dimer formation was included to inform the prescription of 2-methyltetrol oligomerization timescales in WRF-Chem ambient simulation. Reaction rate constants (k) for the THF-diol, triol, and 2-methyltetrol formation (R2–R4) were varied to minimize the sum of squared errors for measured gas-phase products and total OA. The OS formation rate constant (k_{R5}) was fixed at 1.27×10^{-3} $M^{-2}\ s^{-1}$, consistent with WRF-Chem rate constant; this also reduced the number of rate constants requiring fitting, since all other rate constants were treated relative to the OS rate. It is this relative rate that determines the distribution of condensed-phase reaction products[38,52]. Dimer formation (k_{R6}) was set to $0.038 \times k_{R2}$[24]. It should be noted that in previous work, gas-phase 2-MT was not reported, and a much lower C* was used in the model; together, these contributed to a lower k_{MT}/k_{MTS}. In this work, even a k_{MT}/k_{MTS} ratio of ~0.1 fails to reproduce the observed gas-phase 2-MT. Given the available measurement constraints (gas-phase and total organic aerosol mass), a substantially higher reaction rate is therefore required. Best-fit constants are summarized in Supplementary Table 2, with simulations shown in Fig. 2 and Supplementary Figs. 7 and 8.

Note that the formation of oligomers through acid-driven coupling of OS with IEPOX was not explicitly treated like the previous studies[24,31]. There are two reasons for this choice. First, OS dimer is not represented in WRF-Chem. Second, this reaction does not change the total OS but only redistribute the OS monomer to dimer, which are both considered non-volatile. There is no benefit in adding an additional unconstrained parameter for the goal of constraining rate constants for the semi-volatile species that have gas-phase measurement constraints. The formation of tetrol dimers was retained in the box model and used to guide estimation of ambient tetrol oligomerization time scale since the species is represented in WRF-Chem.

THF-diols, triols, and tetrols were treated as semivolatile compounds, of which the saturation vapor concentrations (C^*) at 298K were estimated by the vapor pressure module in a molecular and aerosol property prediction tool UManSysProp[53] (https://doi.org/10.5281/zenodo.594474) following the EVAPORATION method[54]. The estimated C* values along with the input SMILES strings can be found in Supplementary Table 4. The particle-phase fractions of these three semivolatile species were then calculated by Eqn. (2), where C_{OA} is mass concentration of total OA.

$$F_p = \frac{particle}{gas + particle} = \left(1 + \frac{C^*}{C_{OA}}\right)^{-1} \quad (2)$$

First-order gaseous wall-loss rate constants ($k_{wall–IEPOX} = 1.1\times10^{-4} – 4\times10^{-4}\ s^{-1}$) were estimated from IEPOX decay before inorganic seed injection. A typical chamber aerosol wall-loss rate constant ($k_{wall–aerosol} = 1\times10^{-5}\ s^{-1}$) was applied to all aerosol-phase species. The coupled ordinary differential equations

(ODEs) corresponding to the production and/or loss of all gas- and aerosol-phase species were solved and integrated over the 1-h duration following seed injection by MATLAB (R2019b).

WRF-Chem simulations

Third-order reaction rate constants used in WRF-Chem Simulations are reported in Supplementary Table 5.

WRF-Chem description for the southeastern United States

We used the regional WRF-Chem 4.2 model[55,56] to simulate trace gases and aerosols during the summertime (June 20-28, 2013) at 12-km grid spacing for a domain covering 2160 × 2160 km over the SE USA. (Fig. 3 and Supplementary Table 6). The CAM-chem global model[57] provided initial and boundary conditions for trace gases and aerosols. The European Centre for Medium-Range Weather Forecasts Reanalysis version 5 (ERA5) reanalysis data was used to provide meteorological initial and boundary conditions[58] as well as the target fields for nudging. Meteorological and chemical conditions were spun up for 2 days using WRF-Chem followed by two concatenated 2-day simulations where meteorology was reset to the ERA5 reanalysis data every 2 days but traces gases and aerosols were initialized from those at the end of the previous simulation. Gas-phase chemistry is based on the Statewide Air Pollution Research Center (SAPRC-99) mechanism, which includes 211 reactions of 74 gas phase species, 18 of which are free radicals. Inorganic aerosol chemistry, and the evolution of aerosol size distribution and microphysics in WRF-Chem is represented by the Model for Simulating Aerosol Interactions and Chemistry (MOSAIC)[59]. We represent each particle-phase chemical constituent in WRF-Chem by 20 particle size sections ranging from 1 nm to 10 μm for both interstitial and cloud-borne aerosols. Hourly aerosol and trace gas emissions from sources other than biomass burning and biogenic emissions are derived from the United States Environmental Protection Agency's 2014 National Emissions Inventory (NEI2014). Biogenic volatile organic compounds (BVOC) emissions are derived from the latest version of Model of Emissions of Gases and Aerosols from Nature (MEGAN v2.1), coupled within the community land model CLM4 (CLM version 4.0) land surface model in WRF-Chem[60]. SOA formation mechanisms are same as described in Shrivastava et al.[36], with further updates to IEPOX-SOA formation mechanisms as described in this study.

WRF-Chem description for the Amazon rainforest

We used the WRF-Chem model with a 10 km grid spacing covering 1500 × 1000 km around the Manaus urban area in the Amazon with the same configuration (Supplementary Table 6) as described in Shrivastava et al.[39]. The National Centers for Environmental Prediction (NCEP) Climate Forecast System Version 2 (CFSv2) reanalysis data (CFSR)[61] provided the meteorological initial and boundary conditions. Meteorological and chemical conditions were spun up for 2 days using WRF-Chem followed by two concatenated 3-day simulations where meteorology was reset to the CFSR reanalysis data every 2 days, but trace gases and aerosols were initialized from those at the end of the previous simulation. The quasi-

global WRF-Chem simulation for 2014 provided chemical boundary conditions for trace gases and aerosols over the outer domain[62]. Our simulations used detailed SOA parameterizations with additional developments related to IEPOX-SOA as described here. Each particle-phase chemical constituent is represented by 20 size sections as both interstitial and cloud-borne aerosols. Trace gases, aerosols, and clouds are simulated simultaneously with meteorology[63]. Biogenic VOC emissions are predicted using the Model of Emissions of Gases and Aerosols from Nature (MEGAN v 2.1)[63], coupled to the Community Land Model (CLM) land surface model. Due to the large computational costs associated with our SOA parameterizations, we only conducted simulations for 8-day period during Sep 21-29, 2014 with the first 2 days used for model spin-up. However, the results and conclusions from this study likely apply more broadly—over the entire dry season period. The meteorological and chemical boundary conditions, land-surface scheme, and radiation scheme used for configuring the WRF-Chem runs used in this work are listed in Supplementary Table 7. The land surface data and emissions of trace gases and aerosols used for the simulations are further described in detail in Shrivastava et al.[39].

Limitations of the box-model approach

The zero-dimensional box model used here to derive THF-diol, triol, and 2-methyltetrol formation kinetics is intentionally simplified relative to the resistor-model framework implemented in WRF-Chem, and several of its choices merit explicit caveats. First, a constant, experiment-specific γIEPOX was used to reproduce the observed IEPOX decay, rather than an explicit treatment of gas-phase diffusion, surface accommodation, and inorganic–organic phase separation; while this simplification is well justified for the present chamber conditions, it should not be read as evidence that these processes are unimportant more generally, and WRF-Chem retains the fuller resistor-model treatment for the regional-scale simulations. Second, dimer formation in the box model was restricted to the reaction of 2-methyltetrols with IEPOX (R6); coupling of 2-methyltetrol sulfates (organosulfate monomers) with IEPOX to form organosulfate dimers, which has been reported in prior chamber studies, was not included. Because dimer formation was estimated to occur on a timescale of approximately 1000 hours under the conditions of our box-model fits, far longer than the ~1-hour duration of the chamber experiments, this omission is expected to have a negligible effect on the interpretation of the present laboratory dataset, but it means the box model should not be taken as a constraint on ambient dimer (including organosulfate dimer) formation, which can occur over the much longer timescales relevant to the atmosphere. Third, and relatedly, particle-phase organosulfates, including 2-methyltetrol sulfate, have been reported to account for a substantial fraction of organic aerosol mass in some field and chamber studies, underscoring that the ~70% particle-phase mass fraction and its 2-methyltetrol/organosulfate/dimer composition reported here (Fig. 2) reflect the specific conditions of our experiments and should not be interpreted as a complete accounting of IEPOX-derived particulate organosulfate formation more broadly. Finally, the reaction rate constants derived from the box model correspond to RH < 50% and acidic (pH 1.4–1.5) seed aerosol; their extrapolation to the higher-RH, less acidic conditions, and lower condensation sink relevant to the

SOAS and GoAmazon WRF-Chem simulations relies on a scaling assumption drawn from the literature and constitutes an additional source of uncertainty in the regional-scale estimates presented in the main text.

Data availability

The data underlying the main figures are provided as Source Data with this paper. The Vocus CI-IMS-TOF data were generated by Tofwerk AG and are proprietary; they cannot be publicly deposited because of company confidentiality policy. The full raw WRF-Chem output is too large for public deposition. Both datasets are available from the corresponding authors upon reasonable request, subject to Tofwerk AG's approval for the proprietary data, with a response within two weeks.

Code availability

WRF-Chem version 4.2 is publicly available from the National Center for Atmospheric Research (https://www2.mmm.ucar.edu/wrf/users/).

References

1. Hallquist, M. et al. The formation, properties and impact of secondary organic aerosol: current and emerging issues. *Atmos. Chem. Phys.* **9**, 5155–5236 (2009).

2. Shrivastava, M. et al. Recent advances in understanding secondary organic aerosol: Implications for global climate forcing. *Rev. Geophys.* **55**, 509–559 (2017).

3. Li, H. et al. Global biogenic isoprene emissions 2013–2020 inferred from satellite isoprene observations. *Earth Syst. Sci. Data* **17**, 7035–7054 (2025).

4. Guenther, A. et al. Estimates of global terrestrial isoprene emissions using MEGAN (Model of emissions of gases and aerosols from nature). *Atmos. Chem. Phys.* **6**, 3181–3210 (2006).

5. Wennberg, P. O. et al. Gas-phase reactions of isoprene and its major oxidation products. *Chem. Rev.* **118**, 3337–3390 (2018).

6. St. Clair, J. M. et al. Kinetics and products of the reaction of the first-generation isoprene hydroxy hydroperoxide (ISOPOOH) with OH. *J. Phys. Chem. A* **120**, 1441–1451 (2016).

7. Surratt, J. D. et al. Reactive intermediates revealed in secondary organic aerosol formation from isoprene. *Proc. Natl Acad. Sci. USA* **107**, 6640–6645 (2010).

8. Lin, Y.-H. et al. Epoxide as a precursor to secondary organic aerosol formation from isoprene photooxidation in the presence of nitrogen oxides. *Proc. Natl Acad. Sci. USA* **110**, 6718–6723 (2013).

9. Paulot, F. et al. Unexpected epoxide formation in the gas-phase photooxidation of isoprene. *Science* **325**, 730–733 (2009).

10. Budisulistiorini, S. H. et al. Examining the effects of anthropogenic emissions on isoprene-derived secondary organic aerosol formation during the 2013 Southern Oxidant and Aerosol Study (SOAS) at the Look Rock, Tennessee ground site. *Atmos. Chem. Phys.* **15**, 8871–8888 (2015).

11. Jo, D. S. et al. Future changes in isoprene-epoxydiol-derived secondary organic aerosol (IEPOX SOA) under the shared socioeconomic pathways: the importance of physicochemical dependency. *Atmos. Chem. Phys.* **21**, 3395–3425 (2021).

12. Xing, J. et al. Observations and modeling of air quality trends over 1990–2010 across the Northern Hemisphere: China, the United States and Europe. *Atmos. Chem. Phys.* **15**, 2723–2747 (2015).

13. Hu, W. W. et al. Characterization of a real-time tracer for isoprene epoxydiols-derived secondary organic aerosol (IEPOX-SOA) from aerosol mass spectrometer measurements. *Atmos. Chem. Phys.* **15**, 11807–11833 (2015).

14. Xu, L. et al. Effects of anthropogenic emissions on aerosol formation from isoprene and monoterpenes in the southeastern United States. *Proc. Natl Acad. Sci. USA* **112**, 37–42 (2015).

15. Riva, M. et al. Increasing isoprene epoxydiol-to-inorganic sulfate aerosol ratio results in extensive conversion of inorganic sulfate to organosulfur forms: Implications for aerosol physicochemical properties. *Environ. Sci. Technol.* **53**, 8682–8694 (2019).

16. Claeys, M. et al. Formation of secondary organic aerosols through photooxidation of isoprene. *Science* **303**, 1173–1176 (2004).

17. Surratt, J. D. et al. Chemical composition of secondary organic aerosol formed from the photooxidation of isoprene. *J. Phys. Chem. A* **110**, 9665–9690 (2006).

18. Lin, Y.-H. et al. Isoprene epoxydiols as precursors to secondary organic aerosol formation: Acid-catalyzed reactive uptake studies with authentic compounds. *Environ. Sci. Technol.* **46**, 250–258 (2012).

19. Watanabe, A. C., Stropoli, S. J. & Elrod, M. J. Assessing the potential mechanisms of isomerization reactions of isoprene epoxydiols on secondary organic aerosol. *Environ. Sci. Technol.* **52**, 8346–8354 (2018).

20. Frauenheim, M., Offenberg, J., Zhang, Z., Surratt, J. D. & Gold, A. The C5-alkene triol conundrum: Structural characterization and quantitation of isoprene-derived $C_5H_{10}O_3$ reactive uptake products. *Environ. Sci. Technol. Lett.* **9**, 829–836 (2022).

21. Frauenheim, M., Offenberg, J., Zhang, Z., Surratt, J. D. & Gold, A. Chemical composition of secondary organic aerosol formed from the oxidation of semivolatile isoprene epoxydiol isomerization products. *Environ. Sci. Technol.* **58**, 22571–22582 (2024).

22. Zhang, Y. et al. Chemical ionization mass spectrometry: Developments and applications for on-line characterization of atmospheric aerosols and trace gases. *Trends Anal. Chem.* **168**, 117353 (2023).

568 23. Zhang, W., Xu, L. & Zhang, H. Recent advances in mass spectrometry techniques for atmospheric
569 chemistry research on molecular-level. *Mass Spectrom. Rev.* **43**, 1091–1134 (2024).

570 24. Riedel, T. P. et al. Constraining condensed-phase formation kinetics of secondary organic aerosol
571 components from isoprene epoxydiols. *Atmos. Chem. Phys.* **16**, 1245–1254 (2016).

572 25. Zhang, Y. et al. Effect of the aerosol-phase state on secondary organic aerosol formation from the
573 reactive uptake of isoprene-derived epoxydiols (IEPOX). *Environ. Sci. Technol. Lett.* **5**, 167–174 (2018).

574 26. Hu, W. et al. Volatility and lifetime against OH heterogeneous reaction of ambient isoprene-
575 epoxydiols-derived secondary organic aerosol (IEPOX-SOA). *Atmos. Chem. Phys.* **16**, 11563–11580
576 (2016).

577 27. Chen, Y. et al. Heterogeneous hydroxyl radical oxidation of isoprene-epoxydiol-derived methyltetrol
578 sulfates: Plausible formation mechanisms of previously unexplained organosulfates in ambient fine
579 aerosols. *Environ. Sci. Technol. Lett.* **7**, 460–468 (2020).

580 28. Riedel, T. P. et al. Heterogeneous reactions of isoprene-derived epoxides: Reaction probabilities and
581 molar secondary organic aerosol yield estimates. *Environ. Sci. Technol. Lett.* **2**, 38–42 (2015).

582 29. Cole-Filipiak, N. C., O'Connor, A. E. & Elrod, M. J. Kinetics of the hydrolysis of atmospherically
583 relevant isoprene-derived hydroxy epoxides. *Environ. Sci. Technol.* **44**, 6718–6723 (2010).

584 30. Piletic, I. R., Edney, E. O. & Bartolotti, L. J. A computational study of acid catalyzed aerosol reactions
585 of atmospherically relevant epoxides. *Phys. Chem. Chem. Phys.* **15**, 18065 (2013).

586 31. Chen, Y. et al. Applying a phase-separation parameterization in modeling secondary organic aerosol
587 formation from acid-driven reactive uptake of isoprene epoxydiols under humid conditions. *ACS EST Air*
588 **1**, 511–524 (2024).

589 32. Eddingsaas, N. C., VanderVelde, D. G. & Wennberg, P. O. Kinetics and products of the acid-catalyzed
590 ring-opening of atmospherically relevant butyl epoxy alcohols. *J. Phys. Chem. A* **114**, 8106–8113 (2010).

591 33. Zhang, J. et al. New formation and fate of isoprene SOA markers revealed by field data-constrained
592 modeling. *npj Clim. Atmos. Sci.* **6**, 69 (2023).

593 34. D'Ambro, E. L. et al. Chamber-based insights into the factors controlling epoxydiol (IEPOX)
594 secondary organic aerosol (SOA) yield, composition, and volatility. *Atmos. Chem. Phys.* **19**, 11253–
595 11265 (2019).

596 35. Liu, X. et al. Effects of gas–wall interactions on measurements of semivolatile compounds and small
597 polar molecules. *Atmos. Meas. Tech.* **12**, 3137–3149 (2019).

598 36. Shrivastava, M. et al. Anthropogenic extremely low volatility organics (ELVOCs) govern the growth
599 of molecular clusters over the Southern Great Plains during the springtime. *J. Geophys. Res. Atmos.* **129**,
600 e2024JD041212 (2024).

37. Anttila, T., Kiendler-Scharr, A., Tillmann, R. & Mentel, T. F. On the reactive uptake of gaseous compounds by organic-coated aqueous aerosols: Theoretical analysis and application to the heterogeneous hydrolysis of N_2O_5. *J. Phys. Chem. A* **110**, 10435–10443 (2006).

38. Zhang, J. et al. Observationally constrained modeling of the reactive uptake of isoprene-derived epoxydiols under elevated relative humidity and varying acidity of seed aerosol conditions. *ACS Earth Space Chem.* **7**, 788–799 (2023).

39. Shrivastava, M. et al. Tight coupling of surface and in-plant biochemistry and convection governs key fine particulate components over the Amazon rainforest. *ACS Earth Space Chem.* **6**, 380–390 (2022).

40. Octaviani, M. et al. Modeling the size distribution and chemical composition of secondary organic aerosols during the reactive uptake of isoprene-derived epoxydiols under low-humidity condition. *ACS Earth Space Chem.* **5**, 3247–3257 (2021).

41. Ye, J. et al. Near-canopy horizontal concentration heterogeneity of semivolatile oxygenated organic compounds and implications for 2-methyltetrols primary emissions. *Environ. Sci.: Atmos.* **1**, 8–20 (2021).

42. Su, Q. et al. Enhanced isoprene secondary organic aerosol formation with C5-alkene triols newly added to current chemical mechanisms. *ACS EST Air*, doi: 10.1021/acsestair.5c00124 (2025).

43. De Sá, S. S. et al. Contributions of biomass-burning, urban, and biogenic emissions to the concentrations and light-absorbing properties of particulate matter in central Amazonia during the dry season. *Atmos. Chem. Phys.* **19**, 7973–8001 (2019).

44. Lindinger, W. & Jordan, A. Proton-transfer-reaction mass spectrometry (PTR–MS): on-line monitoring of volatile organic compounds at pptv levels. *Chem. Soc. Rev.* **27**, 347 (1998).

45. Wiedensohler, A. et al. Mobility particle size spectrometers: harmonization of technical standards and data structure to facilitate high quality long-term observations of atmospheric particle number size distributions. *Atmos. Meas. Tech.* **5**, 657–685 (2012).

46. Riva, M. et al. Evaluation of a reduced-pressure chemical ion reactor utilizing adduct ionization for the detection of gaseous organic and inorganic species. *Atmos. Meas. Tech.* **17**, 5887–5901 (2024).

47. Tolmachev, A. V. et al. Characterization of ion dynamics in structures for lossless ion manipulations. *Anal. Chem.* **86**, 9162–9168 (2014).

48. Frauenheim, M., Surratt, J. D., Zhang, Z. & Gold, A. Technical note: Improved synthetic routes to *cis*- and *trans*-(2-methyloxirane-2,3-diyl)dimethanol (*cis*- and *trans*-*β*-isoprene epoxydiol). *Atmos. Chem. Phys.* **23**, 7859–7866 (2023).

49. Lee, B. H. et al. An iodide-adduct high-resolution time-of-flight chemical-ionization mass spectrometer: Application to atmospheric inorganic and organic compounds. *Environ. Sci. Technol.* **48**, 6309–6317 (2014).

634 50. Clegg, S. L., Brimblecombe, P. & Wexler, A. S. Thermodynamic model of the system H^+–NH_4^+–
635 SO_4^{2-}–NO_3^-–H_2O at tropospheric temperatures. *J. Phys. Chem. A* **102**, 2137–2154 (1998).

636 51. Wexler, A. S. & Clegg, S. L. Atmospheric aerosol models for systems including the ions H^+, NH_4^+,
637 Na^+, SO_4^{2-}, NO_3^-, Cl^-, Br^- and H_2O. *J. Geophys. Res. Atmos.* **107**, ACH 14-1-ACH 14-14 (2002).

638 52. Budisulistiorini, S. H. et al. Simulating aqueous-phase isoprene-epoxydiol (IEPOX) secondary
639 organic aerosol production during the 2013 Southern Oxidant and Aerosol Study (SOAS). *Environ. Sci.*
640 *Technol.* **51**, 5026–5034 (2017).

641 53. Topping, D. et al. UManSysProp v1.0: an online and open-source facility for molecular property
642 prediction and atmospheric aerosol calculations. *Geosci. Model Dev.* **9**, 899–914 (2016).

643 54. Compernolle, S., Ceulemans, K. & Müller, J.-F. EVAPORATION: a new vapour pressure estimation
644 method for organic molecules including non-additivity and intramolecular interactions. *Atmos. Chem.*
645 *Phys.* **11**, 9431–9450 (2011).

646 55. Fast, J. D. et al. Evolution of ozone, particulates, and aerosol direct radiative forcing in the vicinity
647 of Houston using a fully coupled meteorology-chemistry-aerosol model. *J. Geophys. Res. Atmos.* **111**
648 (2006).

649 56. Grell, G. A. et al. Fully coupled "online" chemistry within the WRF model. *Atmos. Environ.* **39**,
650 6957–6975 (2005).

651 57. Emmons, L. K. et al. The chemistry mechanism in the Community Earth System Model version 2
652 (CESM2). *J. Adv. Model. Earth Syst.* **12**, e2019MS001882 (2020).

653 58. Hersbach, H. et al. The ERA5 global reanalysis. *Q. J. R. Meteorol. Soc.* **146**, 1999–2049 (2020).

654 59. Zaveri, R. A., Easter, R. C., Fast, J. D. & Peters, L. K. Model for simulating aerosol interactions and
655 chemistry (MOSAIC). *J. Geophys. Res. Atmos.* **113** (2008).

656 60. Zhao, C. et al. Sensitivity of biogenic volatile organic compounds to land surface parameterizations
657 and vegetation distributions in California. *Geosci. Model Dev.* **9**, 1959–1976 (2016).

658 61. Saha, S. et al. The NCEP climate forecast system reanalysis. *Bull. Am. Meteorol. Soc.* **91**, 1015–1058
659 (2010).

660 62. Hu, Z. et al. Trans-Pacific transport and evolution of aerosols: evaluation of quasi-global WRF-Chem
661 simulation with multiple observations. *Geosci. Model Dev.* **9**, 1725–1746 (2016).

662 63. Guenther, A. B. et al. The Model of emissions of gases and aerosols from nature version 2.1
663 (MEGAN2.1): an extended and updated framework for modeling biogenic emissions. *Geosci. Model Dev.*
664 **5**, 1471–1492 (2012).

Acknowledgements

Manish Shrivastava was supported by the U.S. Department of Energy (DOE) Office of Science, Office of Biological and Environmental Research (BER) through the Early Career Research Program and, along with Brian Gaudet, DOE BER's Atmospheric System Research (ASR) program. M.P.F., J.D.S. and A.G. were supported by NSF grant AGS 2304669. The Pacific Northwest National Laboratory (PNNL) is operated for the DOE by Battelle Memorial Institute under contract DE-AC06-76RL01830. Computational resources for the WRF-Chem simulations were provided by EMSL (a DOE Office of Science User Facility sponsored by the Office of Biological and Environmental Research located at PNNL).

Author contributions

Conceptualization: Y.C., M.S., P.M., and M.R. Methodology: M.A. and C.G. Software: H.S. Validation: Y.C., M.S., P.M., and M.R. Instrument development: M.Z.K., S.G., U.R., F.L., S.G., V.Y., and M.R. Organic synthesis: M.P.F, R.B., and A.G. Formal analysis: Y.C., M.S., P.M., and M.R. Investigation: Y.C., M.S., P.M., M.P.F., R.L.R, R.B., M.C., L.P., and M.R. Resources: M.Z.K., F.L., A.G., J.D.S., H.H., and M.R. Data curation: Y.C., M.S., P.M., and M.R. WRF-Chem simulations: M.S and B.G. Writing–original draft: Y.C., M.S., P.M., and M.R. Writing–review and editing: all co-authors Supervision: M.R. and M.Z.K. Project administration: M.R. and M.Z.K. Funding acquisition: A.G., H.H., and M.R.

Competing interests

M.R., V.Y., S.Gr., S.G., U.R., F.L. and M.Z.K. work for Tofwerk AG, and M.C. and H.S. work for Aerodyne Research Inc., companies that commercialize the Vocus-IMS mass spectrometer. MOBILion is the exclusive licensee of the SLIM technology for commercialization purposes; Tofwerk has been authorized to implement the proprietary technology in select products. The other authors declare no competing interests.

Additional information

Supplementary information The online version contains supplementary material (Supplementary Figs. 1–14 and Supplementary Tables 1–8).

Correspondence and requests for materials should be addressed to M.R., A.G. or M.Z.K.

Supplementary Files

This is a list of supplementary files associated with this preprint. Click to download.

- SINatCommun.docx